International Journal of Fracture (2005) 134:369–386
DOI 10.1007/s10704-005-3073-1

Multiscale analysis of fracture of carbon nanotubes embedded in composites

DONG-LI SHI[1], XI-QIAO FENG[1,*], HANQING JIANG[2], YONGGANG Y. HUANG[2] and KEH-CHIH HWANG[1]

[1]*Key Lab of Failure Mechanics, Department of Engineering Mechanics, Tsinghua University, Beijing 100084, People's Republic of China*

[2]*Department of Mechanical and Industrial Engineering, University of Illinois at Urbana-Champaign, Urbana, IL 61801, USA*

[*]*Author for correspondence. (E-mail: fengxq@tsinghua.edu.cn)*

Received 25 August 2004; accepted 7 September 2005

Abstract. Due to the enormous difference in the scales involved in correlating the macroscopic properties with the micro- and nano-physical mechanisms of carbon nanotube-reinforced composites, multiscale mechanics analysis is of considerable interest. A hybrid atomistic/continuum mechanics method is established in the present paper to study the deformation and fracture behaviors of carbon nanotubes (CNTs) in composites. The unit cell containing a CNT embedded in a matrix is divided in three regions, which are simulated by the atomic-potential method, the continuum method based on the modified Cauchy–Born rule, and the classical continuum mechanics, respectively. The effect of CNT interaction is taken into account via the Mori–Tanaka effective field method of micromechanics. This method not only can predict the formation of Stone–Wales (5-7-7-5) defects, but also simulate the subsequent deformation and fracture process of CNTs. It is found that the critical strain of defect nucleation in a CNT is sensitive to its chiral angle but not to its diameter. The critical strain of Stone–Wales defect formation of zigzag CNTs is nearly twice that of armchair CNTs. Due to the constraint effect of matrix, the CNTs embedded in a composite are easier to fracture in comparison with those not embedded. With the increase in the Young's modulus of the matrix, the critical breaking strain of CNTs decreases.

Key words: Carbon nanotube, fracture, hybrid atomistic/continuum method, nanocomposite, Stone-Wales transformation.

1. Introduction

Owing to the unique and superior physical and mechanical properties of carbon nanotubes (CNTs), extensive attention has been attracted on synthesis of nanotubes and their various applications, and intense research in this area is sure to continue. The Young's modulus and tensile strength of CNTs are of the orders of 1 TPa and 20 GPa, or in other words, about 5 and 100 times those of steels, respectively (Treacy et al., 1996; Yakobson and Smalley, 1997; Yu et al., 2000). CNTs may also have very large length-to-diameter aspect ratios (say, more than 10,000). These remarkable properties are attributed to the unique quasi-one-dimensional, tubular nanostructure of CNTs. There seems to be sufficient evidences indicating that CNTs should be a very promising candidate as the ideal reinforcing fibers for advanced composites with

high strength and low density, which are, evidently, of paramount interest in aeronautic and astronautic technology, automobile and many other modern industries.

Some encouraging results have been reported in the development of CNT-reinforced composites. For instance, Qian et al. (2000) reported a CNT-reinforced polystyrene with good dispersion and CNT–matrix adhesion. Using only 0.5% CNT reinforcement, the elastic modulus was improved about 40% over that of the matrix and the tensile strength was improved about 25%. Pötschke et al. (2002) investigated the electrical and rheological behaviors of polycarbonate composites reinforced by multi-walled carbon nanotubes (MWCNT). They found a rapid change in the electrical resistivity and complex viscosity at about 2% volume fraction of CNTs due to the electrical and rheological percolation associated with interactions of CNTs. Andrews et al. (1999) dispersed single-walled carbon nanotubes (SWCNT) in isotropic petroleum pitch matrices and found that the tensile strength, elastic modulus, and electrical conductivity of the composite with 5 wt% content of purified SWCNTs are enhanced by about 90%, 150%, and 340%, respectively. Recently, Ruan et al. (2003) reported that the incorporation of 1 wt% MWCNT reinforcement produces a remarkable increase in the tensile strength and elastic modulus for non-drawn UHMWPE composite films of 49.7% and 38% and, more interestingly, enhances significantly both the ductility and the strain energy absorption before fracture. However, a big difference still exists between these improvements and the expectations predicted from theoretical analysis, and there is still a long way to go to make CNT-reinforced composites with superior comprehensive properties and to achieve their extensive applications in industry. Many other studies demonstrated only modest improvement in the strength and stiffness after CNTs are incorporated into polymers (Schadler et al., 1998; Tibbetts and McHugh, 1999; Andrews et al., 1999; Ajayan et al., 2000; Vigolo et al., 2000).

Therefore, it is of great interest to investigate experimentally and theoretically the deformation and fracture behaviors of CNT-reinforced composites at nano, micro to macro scales and to examine the factors that influence their mechanical properties (Wagner et al., 1998; Lourie et al., 1998; Lourie and Wagner 1999; Bower et al., 1999; Fisher et al., 2002; Watts and Hsu, 2003; Shi et al., 2004a, b; Buryachenko and Roy, 2005). Wagner et al. (1998) and Lourie et al. (1998, 1999) reported excellent interfaces between CNTs and polymer matrix. Qian et al. (2000) found that CNT breaking was a preferred process during cracking of CNT-reinforced films. From *in situ* TEM observation, Watts and Hsu (2003) found that the external force can be effectively transferred to nanotubes and that embedded CNTs delay polymer film cracking via nanotube stretching and pulling out. Recently, Xia et al. (2003) observed three reinforcing mechanisms of CNTs: crack deflection at the CNT/matrix interface, crack bridging by CNTs, and CNT pullout on the fracture surfaces. Based on shell theory, Ru (2001) studied the buckling of a double-walled CNT embedded in an elastic matrix under axial compression. Liu and Chen (2003) and Hu et al. (2005) evaluated the effective mechanical properties of CNT-reinforced composites using a nanoscale representative volume element (RVE) based on continuum mechanics and using the finite element method (FEM). Marc et al. (2003) elucidated the nature of the interaction of CNTs and matrix via molecular dynamics simulations. Odegard et al. (2003) presented a method for linking atomistic simulations of nano-structured materials to continuum models of the corresponding bulk materials. They gave a

constitutive modeling of nanotube-reinforced polymer composites. More recently, Shi et al. (2004b) investigated the relationship between the effective properties and the microstructures of CNT composites, and found that agglomeration and waviness of CNTs have significant influences on the effective elastic moduli. In addition, Shi et al. (2004a) stated that the elastic property of the interphase between CNTs and the matrix plays an insignificant role in the stiffening effect of CNTs on the elastic moduli of composites, though the interface adhesion may influence the strength seriously. However, there is as yet a lack of investigation on the defect nucleation and fracture mechanisms of CNTs embedded in composites.

The present paper is aimed to study the deformation, defect nucleation, and fracture of CNTs embedded in a polymer composite. A multiscale mechanics method is developed, which combines both the continuum mechanics and atomic-potential. The unit cell for a CNT embedded in a matrix is divided into three zones, which are dealt with in different manners according to their deformation features. The critical strains for Stone–Wales defect nucleation and breaking of CNTs are calculated, and the factors that influence the fracture behaviors are examined. The critical strains of defect nucleation and fracture are sensitive to the chiral angle but almost independent of the diameter of the CNT. It is also found that due to the constraint effect of matrix, the CNTs embedded in a composite are much easier to fracture than those not embedded.

2. Multiscale mechanics method for CNTs in composites

Due to the enormous difference in scales involved in correlating the macroscopic properties with the microscopic physical mechanisms of nanostructured materials, multiscale analysis is necessary (see, e.g., Shenoy et al., 1999; Curtin and Miller, 2003; Ghoniem et al., 2003). We adopt here a multiscale mechanics method to study the deformation and fracture behaviors of CNT-reinforced composites. Consider a straight SWCNT embedded in a matrix and subjected to a uniform stress in the far field, as shown in Figure 1. Assume that the interface between the CNT and matrix is perfectly bonded and that there is no residual strain in the composite. In our hybrid atomistic/continuum method, the unit cell in Figure 1 is divided into three zones, A, B and C, which are dealt with in different manners according to their deformation features and the numbers of atoms in them:

(i) A local subregion A is specified in the CNT, where Stone–Wales transformation and fracture will be assumed to initiate. The process of defect nucleation and evolution depends strongly on the directions and lengths of individual C—C bonds in this local region. Therefore, an atomistic method based on the Tersoff–Brenner potential is employed to determine the positions of all the atoms in this region by minimizing the total energy of the atomic system either before or after the defect nucleation (Jiang et al., 2004).

(ii) The region B covers all the atoms outside the local region A of the CNT. The positions of the atoms in B are insensitive to the defect and almost identical to those in a uniformly deformed, defectless CNT, provided that the size of A is large enough. The region B remains approximately the hexagonal lattice structure. Therefore, the positions of atoms in B can be calculated by

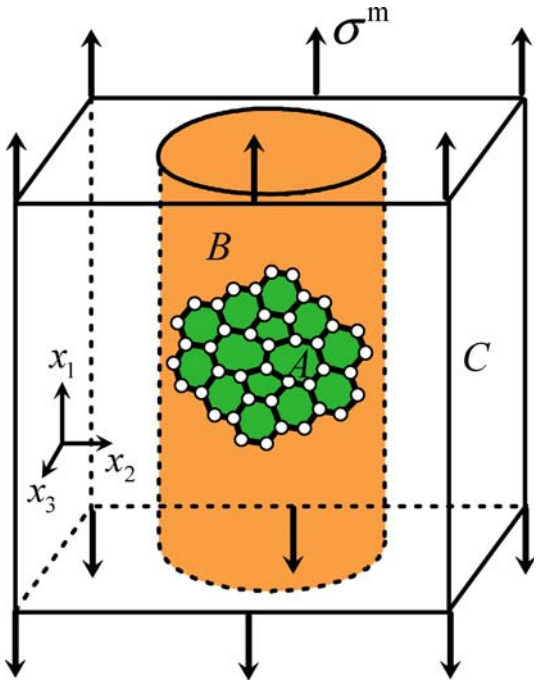

Figure 1. Multiscale analysis model for a CNT-reinforced composite.

using the continuum medium method based on the modified Cauchy–Born rule (Zhang et al., 2002a, b).

(iii) Generally, the polymer matrix around the CNT has an atomistic system much larger than the CNT, and generally does not have a regular lattice. Perfect adhesion is assumed between the CNTs and the matrix, without considering the effect of interphase. Therefore, the polymer matrix region *C* in the unit cell is simulated by a continuum medium in order to account for the interaction of CNTs via a micromechanics method.

This multiscale method combines the advantages of both continuum mechanics and atomic-potential methods. The classical continuum mechanics provides a straightforward approach for estimating the macroscopically averaged or effective properties of deformation and fracture of composites, but cannot predict defect nucleation and fracture at nanoscale. Atomistic studies such as molecular dynamic simulation have been playing an increasingly significant role in studying the physical process occurred in nanosystems such as CNTs. However, atomistic studies are too computationally intensive for CNT-reinforced polymer composites of current interest. It will be shown that the present multiscale method is efficient for simulating the nanoscale fracture process occurred in a composite. The details of this method will be described in the following sections.

2.1. Tersoff–brenner potential

In the combined atomistic/continuum method of this paper, we use the Tersoff–Brenner potential (Brenner, 1990) to simulate the defect nucleation and fracture of CNTs. The multi-body interatomic potential for C—C bonds are expressed as

$$V(r_{ij}) = V_{\mathrm{R}}(r_{ij}) - B_{ij} V_{\mathrm{A}}(r_{ij}), \tag{1}$$

where r_{ij} is the bond length between two carbon atoms i and j, $V_{\mathrm{R}}(r_{ij})$ and $V_{\mathrm{A}}(r_{ij})$ are the repulsive and attractive pair terms given by

$$\begin{aligned} V_{\mathrm{R}}(r) &= \tfrac{1}{S-1} D^{(e)} f_{\mathrm{c}}(r) \exp\left[-\sqrt{2S}\beta(r - R^{(e)})\right], \\ V_{\mathrm{A}}(r) &= \tfrac{S}{S-1} D^{(e)} f_{\mathrm{c}}(r) \exp\left[-\sqrt{\tfrac{2}{S}}\beta(r - R^{(e)})\right], \end{aligned} \tag{2}$$

which depend only on the distance of the two atoms. The parameters $D^{(e)}, S, \beta$ and $R^{(e)}$ have been determined from the known physical properties of carbon, graphite and diamond as $D^{(e)} = 6.0\,\mathrm{eV}$, $S = 1.22$, $\beta = 21\,\mathrm{nm}^{-1}$, and $R^{(e)} = 0.1390\,\mathrm{nm}$. $f_c(r)$ in Equation (2) is a smooth cut-off function which limits the range of the potential to the close neighborhood of each atom, i.e., it damps the interatomic interactions smoothly down to zero from the first to the second neighboring shells. It is expressed as

$$f_{\mathrm{c}}(r) = \begin{cases} 1, & (r \leqslant R^{(1)}), \\ \frac{1}{2}\left\{1 + \cos\left[\frac{\pi(r - R^{(1)})}{R^{(2)} - R^{(1)}}\right]\right\}, & (R^{(1)} < r \leqslant R^{(2)}), \\ 0, & r > R^{(2)} \end{cases} \tag{3}$$

with $R^{(1)} = 0.17\,\mathrm{nm}$ and $R^{(2)} = 0.2\,\mathrm{nm}$ being the effective cut-off ranges of the potential.

The term B_{ij} in Equation (1) represents a multi-body coupling effect, i.e., the contribution of other atoms to the i—j bond, and is given by

$$B_{ij} = \left[1 + \sum_{k(\neq i,j)} G(\theta_{ijk}) f_{\mathrm{c}}(r_{ik})\right]^{-\delta}, \tag{4}$$

where θ_{ijk} is the angle between the bonds $i - j$ and $i - k$, the function $G(\theta_{ijk})$ is defined as

$$G(\theta_{ijk}) = a_0 \left[1 + \frac{c_0^2}{d_0^2} - \frac{c_0^2}{d_0^2 + (1 + \cos\theta_{ijk})^2}\right] \tag{5}$$

with $\delta = 0.500$, $a_0 = 0.00020813$, $c_0 = 330$, and $d_0 = 3.5$ (Brenner, 1990).

2.2. Uniform deformation before defect nucleation

The Cauchy–Born rule (Born and Huang, 1954) is an extensively adopted kinematic assumption for linking the deformation of an atomic system to that of a continuum. The Cauchy–Born rule states that for an atomic structure subjected to a homogeneous deformation, each atom moves according to a single mapping from the initial to the deformed configurations. It is important to point out that the Cauchy–Born rule holds only for centrosymmetric lattice structures. Therefore, the Cauchy–Born rule must be modified when it is used to simulate the deformation of CNTs with hexagonal lattice structure, which does not possess a centrosymmetry. By modifying the Cauchy–Born rule, Zhang et al. (2002a, b) developed an atomic potential-based continuum method for considering the uniform deformation of a CNT before Stone–Wale defect nucleation.

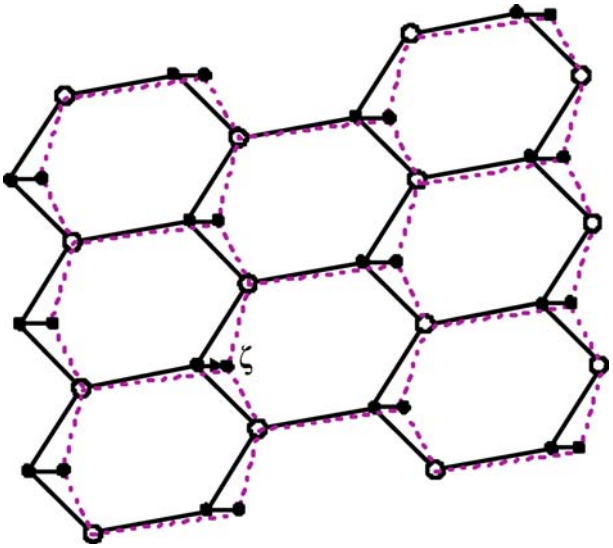

Figure 2. Decomposition of a hexagonal lattice to two triangular sub-lattices.

We assume that the considered CNT possesses a perfect hexagonal lattice structure and has no defect before loading. At lower tensile strains, the CNT will undergo uniform elastic deformation, and no Stone–Wales defect occurs. A non-centrosymmetric, hexagonal lattice structure can be decomposed into two triangular sub-lattices, marked respectively by solid and open circles in Figure 2 (Jiang et al., 2003). Each sub-lattice has a centrosymmetry and therefore follows the Cauchy–Born rule. Before defect appearance, each sub-lattice undergoes uniform deformation. For any two atoms i and j in the same sub-lattice, the vector $\mathbf{r}_{ij}$ from i to j in the deformed configuration is related to the corresponding vector $\mathbf{r}_{ij}^{(0)}$ in the initial, undformed configuration by

$$\mathbf{r}_{ij} = \mathbf{F} \cdot \mathbf{r}_{ij}^{(0)}, \tag{6}$$

where $\mathbf{F} = \partial \mathbf{x} / \partial \mathbf{X}$ is the deformation gradient, $\mathbf{x}$ and $\mathbf{X}$ denote the positions of the same material point in the initial and the deformed configurations, respectively.

However, the two sub-lattices may undergo a relative translation vector $\boldsymbol{\zeta}$, which represents an internal degree of freedom for the hexagonal lattice structure and remains to be determined by enforcing the equilibrium of atoms. No relative rotation is possible between the two sub-lattice. Therefore, for two atoms i and j in the two different sub-lattices, the vector $\mathbf{r}_{ij}$ after deformation is expressed as

$$\mathbf{r}_{ij} = \mathbf{F} \cdot \mathbf{r}_{ij}^{(0)} + \boldsymbol{\zeta}. \tag{7}$$

Thus, the energy of the atomic system obtained from the interatomic potential in Equation (1) depends on both $\mathbf{F}$ and $\boldsymbol{\zeta}$. The strain energy density can be written as

$$W(\mathbf{F}, \boldsymbol{\zeta}) = \frac{1}{2\Omega} \sum V\left(r_{ij}\right), \tag{8}$$

where Ω is the surface area of CNT. By minimizing the energy W in Equation (8) under a given $\mathbf{F}$,

$$\frac{\partial W(\mathbf{F}, \boldsymbol{\zeta})}{\partial \boldsymbol{\zeta}} = 0, \tag{9}$$

one can determine the shift vector $\boldsymbol{\zeta} = \boldsymbol{\zeta}(\mathbf{F}, \boldsymbol{\zeta})$ in terms of $\mathbf{F}$, and thus the strain energy density can be rewritten as $W = W(\mathbf{F}, \boldsymbol{\zeta}(\mathbf{F}))$. Then, the energy of the CNT before defect nucleation can be determined and denoted as $E_{\text{perfect}}(\mathbf{F})$, which is a function of the deformation gradient $\mathbf{F}$.

2.3. Combined atomistic/continuum method for defect nucleation

Our attention is focused on the Stone–Wales defect as it appears to be the lowest energy defect possible in a perfect CNT. When the tensile strain reaches a critical value, a Stone–Wales or pyracylene transformation will occur as a result of 90° rotation of a C—C bond that turns four carbon hexagons, (6-6-6-6), into two pentagons and two heptagons, (5-7-7-5). Nardelli et al. (1998a, b, 2000) and Yakobson et al. (1996, 1998) studied by molecular dynamics simulations the fracture of CNTs at high temperature and found that Stone–Wales defect is a typical mechanism for fracture of CNTs under tension.

A hybrid atomistic/continuum mechanics method is adopted here to calculate the critical strains of Stone–Wales defect nucleation and breaking of SWCNTs with different chiral angles and diameters. As aforementioned, a CNT is divided into two parts that are dealt with by different methods. First, the influence of the Stone–Wales transformation is assumed reasonably to be limited mainly in a local region A around the defect, as shown in Figure 3. The positions of the atoms and the energy of the bonds in this region are dependent strongly upon the defect. Continuum mechanics method is invalid in this region, and an atomic-potential method has to be used to determine when a Stone–Wales transformation will occur and which C—C bond will rotate. It will be shown in the sequel that the size of A does not influence the calculation results provided that it is large enough. Second, the atoms far from the defect feel little impact from the defect nucleation and undergo almost uniform deformation. Therefore, we assume that the positions of all the atoms in the B region in Figure 3 are not influenced by the defect and can still be determined by the continuum mechanics method based on the modified Cauchy–Born rule, as described in Section 2.2 (Zhang et al., 2002a, b). The positions of atoms in the innermost layer of the region B, marked by the grey circles in Figure 3, are used as the boundary condition of the atomistic simulation in the region A.

Refer to a planar Cartesian coordinate system (o-xy), as shown in Figure 3. Let N denote the total number of the atoms in the region A. The coordinates of the atoms in this region are expressed as $(x_1, y_1), (x_2, y_2), \ldots, (x_N, y_N)$ respectively, which need to be determined by the energy method. It should be noted that to calculate the energy of the C—C bonds, the coordinates of the atoms in the cylindrical configuration should be determined first by the transformation relation from the Cartesian coordinate system to the cylindrical coordinate system, as described by Jiang et al. (2003). The energy stored in the region A can be written as the summation of all the C—C bonds:

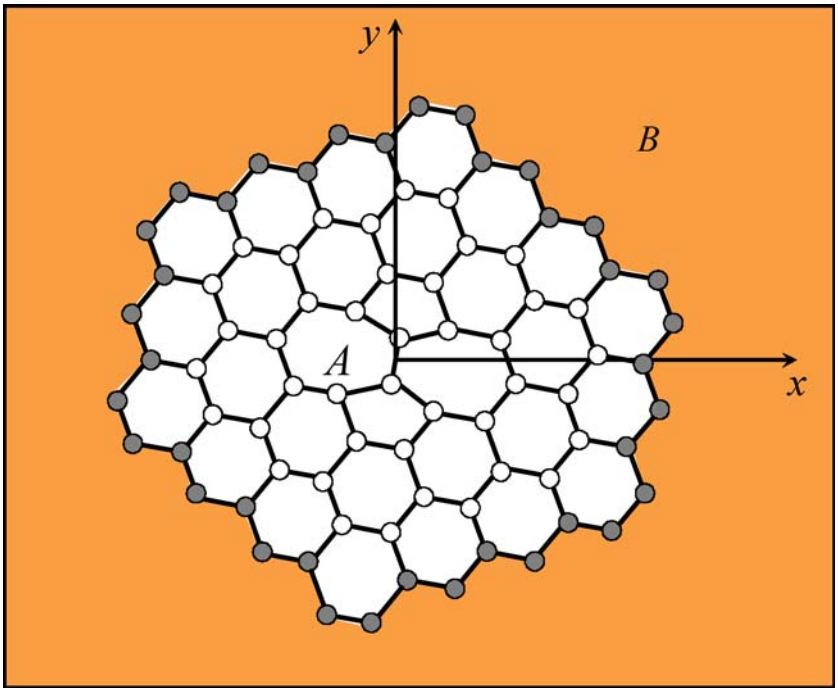

Figure 3. Hybrid atomistic/continuum mechanics model for simulating defect nucleation and fracture of CNTs.

$$E = E(x_1, y_1, x_2, y_2, \ldots, x_N, y_N) = \sum_{\alpha=1}^{N_b} V_\alpha, \tag{10}$$

where N_b is the total number of the bonds in A, and V_α is the energy of the αth bond, determined from the Tersoff–Brenner potential in Equation (1). The energy E of the system is a function of the $2N$ unknown coordinate parameters.

The equilibrium condition requires that the derivatives of the energy E with respect to the coordinates $(x_\alpha, y_\alpha)(\alpha = 1, 2, \ldots, N)$ vanish under the given loading condition, that is,

$$\frac{\partial E}{\partial x_i} = 0, \qquad \frac{\partial E}{\partial y_i} = 0, \quad (\alpha = 1, 2, \ldots, N). \tag{11}$$

Then all the positions of the N atoms in the region A can be determined by solving the $2N$ equations in Equation (11).

Clearly, this atomistic method is valid for both the configurations before and after defect nucleation. Let E_{perfect} signify the energy stored in the A region with regular hexagonal lattice structure, and E_{defect} that with a (5-7-7-5) defect. First, we calculate the uniform deformation of CNTs under uniaxial tension by using the above multiscale method. The calculation results show that the atom positions and the corresponding energy E_{perfect} before Stone–Wales transformation are identical to those predicted from the modified Cauchy–Born rule (Zhang et al., 2002a, b). The Stone–Wales transformation (e.g., 90° rotation of a C—C bond about their mutual bond centre) does not cause a change of the total number of bonds in the region A.

Both E_{perfect} and E_{defect} depend on the deformation gradient **F** in the CNT, which will be determined as a function of the applied stress applied on the composite by using a micromechanics method. At infinitesimal strain, E_{defect} is always larger than E_{perfect}, and therefore the CNT undergoes uniform deformation. As the strain increases, both E_{perfect} and E_{defect} increase, but the latter changes more slowly. After the strain reaches a critical value ε_{SW}, E_{defect} will become smaller than E_{perfect}, the Stone–Wales transformation becomes more favorable energetically, and then defect nucleation may occur.

After the defect forms, the deformation of the CNT is still stable and no bond breaking occurs until the tensile strain reaches another critical value, $\varepsilon_{\text{break}}$. The critical strain $\varepsilon_{\text{break}}$ of fracture can also be obtained from the present hybrid atomistic/continuum mechanics method. In the Tersoff–Brenner potential, they use the three-regime cut-off function $f_c(r)$ in Equation (3) to describe the interactive force between two carbon atoms. In our calculation, however, no cut-off function has been introduced for bond breaking. In other words, the bond between two neighboring atoms is always thought to exist during the total deformation process even when their spacing is very large and their interactive force is very weak. A bond is considered to have broken when its length is larger than 0.2 nm. Therefore, the strain under which the deformation of the Stone–Wales (5-7-7-5) defect system becomes unstable or localized is defined as the breaking strain, $\varepsilon_{\text{break}}$. Strain localization initiated by a defect is generally a typical stage of deformation before the final rupture of a CNT.

The effect of the specified size of the subregion A is first examined in our calculation. The larger the region A, the more accurate the calculation results of the energy stored in the system. Therefore, the region A should contain a sufficient number of atoms in order to ensure that the hybrid atomistic/continuum method leads to sufficiently accurate results. We compare four different sizes of A, which contain one, two, three and four layers of atoms surrounding the Stone–Wales (5-7-7-5) defect, respectively. The corresponding total atom numbers in A are 42, 80, 130 and 192, respectively. It is found that both the obtained critical strains of defect nucleation and breaking approach to constants with the increase in the size of A. The relative difference between the critical strains obtained from the systems containing 130 and 192 atoms is less than 5%. According to our numerical calculations, a subregion A containing 130 atoms (three layers) seems suitable to achieve a balance of the accuracy of results and the simplicity of calculation. For a long CNT in a composite, multiple defects may nucleate at different sites. The interaction between defects has not been considered in this study.

2.4. Effect of CNT interaction

The interaction of CNTs in a composite may influence their deformation and fracture behaviors. Many methods (e.g., self-consistent method, differential method, and Mori–Tanaka method) have been established in micromechanics for considering the interaction effect. To calculate the deformation gradient **F** in a CNT as a function of the applied stress $\boldsymbol{\sigma}^0$, we adopt the Mori–Tanaka method (Mori and Tanaka, 1973) because of its simplicity and accuracy even at a high volume fraction of the reinforcing phase. For convenience, the CNTs are considered as straight fibers embedded in

the composite. Curved CNTs can also be analyzed by using the unit-cell model suggested by Shi et al. (2004b).

To estimate the interaction effect of distributed inclusions in composites, the Mori–Tanaka method assumes that each inclusion is placed in an infinite pristine matrix and that the far-field stress $\boldsymbol{\sigma}^0$ is replaced by the average stress $\boldsymbol{\sigma}^{\mathrm{m}}$ in the matrix (Mori and Tanaka, 1973). $\boldsymbol{\sigma}^{\mathrm{m}}$ can be written as (Weng, 1984)

$$\boldsymbol{\sigma}^{\mathrm{m}} = \boldsymbol{\sigma}^0 + \tilde{\boldsymbol{\sigma}} = \mathbf{L}^{\mathrm{m}} : \left(\boldsymbol{\varepsilon}^0 + \tilde{\boldsymbol{\varepsilon}}\right) = \mathbf{L}^{\mathrm{m}} : \boldsymbol{\varepsilon}^{\mathrm{m}}, \tag{12}$$

where $\tilde{\boldsymbol{\sigma}}$ denotes the average perturbed stress in the matrix due to the presence of CNTs, $\boldsymbol{\varepsilon}^{\mathrm{m}}$ and $\mathbf{L}^{\mathrm{m}}$ are the average strain and the elastic stiffness tensor of the matrix, respectively, and $\boldsymbol{\varepsilon}^0 = (\mathbf{L}^{\mathrm{m}})^{-1} : \boldsymbol{\sigma}^0$. The average stress in the CNTs can be expressed as

$$\begin{aligned} \boldsymbol{\sigma}^{\mathrm{CNT}} &= \boldsymbol{\sigma}^0 + \tilde{\boldsymbol{\sigma}} + \boldsymbol{\sigma}' = \mathbf{L}^{\mathrm{CNT}} : \left(\boldsymbol{\varepsilon}^0 + \tilde{\boldsymbol{\varepsilon}} + \boldsymbol{\varepsilon}'\right) \\ &= \mathbf{L}^{\mathrm{m}} : \left(\boldsymbol{\varepsilon}^0 + \tilde{\boldsymbol{\varepsilon}} + \boldsymbol{\varepsilon}' - \boldsymbol{\varepsilon}^*\right) = \mathbf{L}^{\mathrm{CNT}} : \boldsymbol{\varepsilon}^{\mathrm{CNT}}, \end{aligned} \tag{13}$$

where $\boldsymbol{\varepsilon}^{\mathrm{CNT}}$ and $\mathbf{L}^{\mathrm{CNT}}$ denote the average strain and the elastic stiffness tensor of the CNTs, respectively, $\boldsymbol{\sigma}' = \boldsymbol{\sigma}^{\mathrm{CNT}} - \boldsymbol{\sigma}^{\mathrm{m}}$ is the difference in the average stresses of the two phases, and $\boldsymbol{\varepsilon}^*$ serves as the Eshelby eigenstrain (Mura, 1987).

The average theorems of stresses and strains require that

$$\boldsymbol{\sigma}^0 = (1-c)\boldsymbol{\sigma}^{\mathrm{m}} + c\boldsymbol{\sigma}^{\mathrm{CNT}}, \quad \boldsymbol{\varepsilon}^0 = (1-c)\boldsymbol{\varepsilon}^{\mathrm{m}} + c\boldsymbol{\varepsilon}^{\mathrm{CNT}}, \tag{14}$$

where c is the volume fraction of the CNTs. Substituting Equations (12) and (13) into Equation (14) leads to

$$\tilde{\boldsymbol{\sigma}} = -c\boldsymbol{\sigma}', \quad \tilde{\boldsymbol{\varepsilon}} = -c\boldsymbol{\varepsilon}'. \tag{15}$$

Substituting the Eshelby's relation $\boldsymbol{\varepsilon}' = \mathbf{S} : \boldsymbol{\varepsilon}^*$ (Mura, 1987) and Equation (15) into Equation (13), where $\mathbf{S}$ is the Eshelby tensor, one has

$$\tilde{\boldsymbol{\varepsilon}} = -c\left(\boldsymbol{\varepsilon}' - \boldsymbol{\varepsilon}^*\right) = -c\left(\mathbf{S} - \mathbf{I}\right) : \boldsymbol{\varepsilon}^*. \tag{16}$$

Then from Equations (13), (15) and (16), the average strain of the CNTs reads

$$\boldsymbol{\varepsilon}^{\mathrm{CNT}} = \boldsymbol{\varepsilon}^0 + \tilde{\boldsymbol{\varepsilon}} + \boldsymbol{\varepsilon}' = \boldsymbol{\varepsilon}^0 + [c\mathbf{I} + (1-c)\,\mathbf{S}] : \boldsymbol{\varepsilon}^*, \tag{17}$$

with

$$\boldsymbol{\varepsilon}^* = -\left\{\left(\mathbf{L}^{\mathrm{CNT}} - \mathbf{L}^{\mathrm{m}}\right) : [c\mathbf{I} + (1-c)\,\mathbf{S}] + \mathbf{L}^{\mathrm{m}}\right\}^{-1} : \left(\mathbf{L}^{\mathrm{CNT}} - \mathbf{L}^{\mathrm{m}}\right) : \boldsymbol{\varepsilon}^0. \tag{18}$$

The CNTs are assumed to be transversely isotropic elastic. Their elastic stiffness tensor is written as

$$\begin{Bmatrix} \sigma_{11} \\ \sigma_{22} \\ \sigma_{33} \\ \sigma_{23} \\ \sigma_{13} \\ \sigma_{12} \end{Bmatrix} = \begin{bmatrix} n_{\mathrm{r}} & l_{\mathrm{r}} & l_{\mathrm{r}} & 0 & 0 & 0 \\ l_{\mathrm{r}} & k_{\mathrm{r}}+m_{\mathrm{r}} & k_{\mathrm{r}}-m_{\mathrm{r}} & 0 & 0 & 0 \\ l_{\mathrm{r}} & k_{\mathrm{r}}-m_{\mathrm{r}} & k_{\mathrm{r}}+m_{\mathrm{r}} & 0 & 0 & 0 \\ 0 & 0 & 0 & m_{\mathrm{r}} & 0 & 0 \\ 0 & 0 & 0 & 0 & p_{\mathrm{r}} & 0 \\ 0 & 0 & 0 & 0 & 0 & p_{\mathrm{r}} \end{bmatrix} \begin{Bmatrix} \varepsilon_{11} \\ \varepsilon_{22} \\ \varepsilon_{33} \\ 2\varepsilon_{23} \\ 2\varepsilon_{13} \\ 2\varepsilon_{12} \end{Bmatrix}, \tag{19}$$

where n_r, l_r, k_r, m_r and p_r are Hill's elastic parameters (Hill, 1964). Specifically, k_r is the plane-strain bulk modulus normal to the axial direction, n_r is the uniaxial tension modulus in the axial direction, l_r is the associated cross modulus, m_r and p_r are the shear moduli in planes normal and parallel to the CNT direction, respectively.

The elastic tensor of the matrix, which is assumed isotropic, can be written as

$$L^m_{ijkl} = \lambda_m \delta_{ij}\delta_{kl} + \mu_m \left(\delta_{ik}\delta_{jl} + \delta_{il}\delta_{jk}\right), \tag{20}$$

where λ_m and μ_m are the Lame constants.

From Equation (18), one gets

$$\begin{bmatrix} D_1 & 1 & 1 \\ 1 & D_2 & D_3 \\ 1 & D_3 & D_2 \end{bmatrix} \begin{Bmatrix} \varepsilon_1^0 \\ \varepsilon_2^0 \\ \varepsilon_3^0 \end{Bmatrix} + \begin{bmatrix} B_1 & B_2 & B_3 \\ B_4 & B_5 & B_6 \\ B_7 & B_8 & B_9 \end{bmatrix} \begin{Bmatrix} \varepsilon_1^* \\ \varepsilon_2^* \\ \varepsilon_3^* \end{Bmatrix} = 0, \tag{21}$$

where

$$\begin{aligned}
D_1 &= \frac{n_r - \lambda_m - 2\mu_m}{l_r - \lambda_m}, \\
D_2 &= \frac{k_r + m_r - \lambda_m - 2\mu_m}{l_r - \lambda_m}, \\
D_3 &= \frac{k_r - m_r - \lambda_m}{l_r - \lambda_m}, \\
D_4 &= \frac{\lambda_m + 2\mu_m}{l_r - \lambda_m}, \\
D_5 &= \frac{\lambda_m}{l_r - \lambda_m}, \\
B_1 &= cD_1 + D_4 + \frac{(1-c)\nu_m}{1-\nu_m}, \\
B_2 = B_3 &= c + D_5 + \frac{1-c}{2(1-\nu_m)}, \\
B_4 = B_7 &= c + D_5 + \frac{\nu_m (1-c)(D_2 + D_3)}{2(1-\nu_m)}, \\
B_5 = B_9 &= cD_2 + D_4 + \frac{(1-c)[4\nu_m D_3 - D_3 + D_2(5-4\nu_m)]}{8(1-\nu_m)}, \\
B_6 = B_8 &= cD_3 + D_5 + \frac{(1-c)[4\nu_m D_2 - D_2 + D_3(5-4\nu_m)]}{8(1-\nu_m)},
\end{aligned} \tag{22}$$

with ν_m being the Poisson's ratio of the matrix.

In the case of uniaxial tension along the axial direction (x_1) of the CNT (Figure 1), one has $\varepsilon_2^0 = \varepsilon_3^0 = -\nu_m \varepsilon_1^0$. Then, it is easy to solve from Equation (21) that the eigenstrains $\boldsymbol{\varepsilon}^*$ in the CNT can be written in terms of the applied strain $\boldsymbol{\varepsilon}^0$ as

$$\varepsilon_1^* = \Delta_1 \varepsilon_1^0, \quad \varepsilon_2^* = \Delta_2 \varepsilon_1^0, \quad \varepsilon_3^* = \Delta_3 \varepsilon_1^0, \tag{23}$$

where Δ_1, Δ_2, and Δ_3 are functions of B_i and D_i. From Equation (17), one gets the strain of the CNT as a function of the applied strain as

$$\begin{aligned}
\varepsilon_1^{\mathrm{CNT}} &= (1 + c\Delta_1)\,\varepsilon_1^0, \\
\varepsilon_2^{\mathrm{CNT}} &= \left\{ -\nu_{\mathrm{m}} + \frac{\nu_{\mathrm{m}}(1-c)}{2(1-\nu_{\mathrm{m}})}\Delta_1 + \left[c + \frac{(5-4\nu_{\mathrm{m}})(1-c)}{8(1-\nu_{\mathrm{m}})} \right] \Delta_2 + \frac{(4\nu_{\mathrm{m}}-1)(1-c)}{8(1-\nu_{\mathrm{m}})}\Delta_3 \right\} \varepsilon_1^0, \\
\varepsilon_3^{\mathrm{CNT}} &= \left\{ -\nu_{\mathrm{m}} + \frac{\nu_{\mathrm{m}}(1-c)}{2(1-\nu_{\mathrm{m}})}\Delta_1 + \frac{(4\nu_{\mathrm{m}}-1)(1-c)}{8(1-\nu_{\mathrm{m}})}\Delta_2 + \left[c + \frac{(5-4\nu_{\mathrm{m}})(1-c)}{8(1-\nu_{\mathrm{m}})} \right] \Delta_3 \right\} \varepsilon_1^0.
\end{aligned} \tag{24}$$

Finally, the ratio between the circumferential and longitudinal tensile strains of the CNT is obtained as

$$\frac{\varepsilon_{2(3)}^{\mathrm{CNT}}}{\varepsilon_1^{\mathrm{CNT}}} = \frac{(c-1)\,E_{\mathrm{m}}\nu_{\mathrm{m}} + l_{\mathrm{r}}(\nu_{\mathrm{m}}+1)[-1+c(2\nu_{\mathrm{m}}-1)]}{E_{\mathrm{m}}(1-c) + 2k_{\mathrm{r}}\left[1+\nu_{\mathrm{m}} - c\left(2\nu_{\mathrm{m}}^2 + \nu_{\mathrm{m}} - 1\right)\right]}. \tag{25}$$

The above result from the Mori–Tanaka, i.e., Equation (25), is introduced in the hybrid atomistic/continuum method as the boundary condition of CNTs to account for the constraint effect of the matrix as well as the interaction effect on the deformation and fracture behaviors of the CNTs. It should be mentioned that the tensile stress–strain relation of a CNT is nonlinear, especially for a high tensile strain before defect nucleation or fracture. The nonlinear constitutive relation of CNTs under tension can be calculated by using the hybrid atomistic/continuum method described in Section 2.2 (for more detail, see Shi et al., 2004c). Therefore, the Hill's elastic parameters of CNTs used in Equation (25) are not constants but functions of the applied tensile strain. We do not introduce any fitting parameters for the elastic properties of CNTs but determine the elastic parameters directly from the present model based on the Tersoff–Brenner potential. Thus, the defect nucleation and fracture process of CNTs in composite can be simulated by the present multiscale mechanics method. In what follows, we will consider, for illustration, the special case of uniaxial tension. Other loadings such as twisting, shearing or complex loading can also be analyzed similarly.

3. Results and analysis

3.1. Dependence of stone–wales transformation on the chiral angle and diameter

Nardelli et al. (1998a, b, 2000) and Yakobson et al. (1996, 1997, 1998) studied by molecular dynamics simulations the fracture of CNTs at high temperature and obtained the critical strain of Stone–Wales transformation subjected to uniaxial tension. Here, we calculate the critical strains of defect nucleation and fracture of CNTs embedded in a matrix by using our multiscale mechanics model. The dependence of the critical strains on the chiral angles and diameters of CNTs are first examined. The following twelve representative CNTs with different chiral angles and diameters are chosen as examples, which can be classified into four groups:

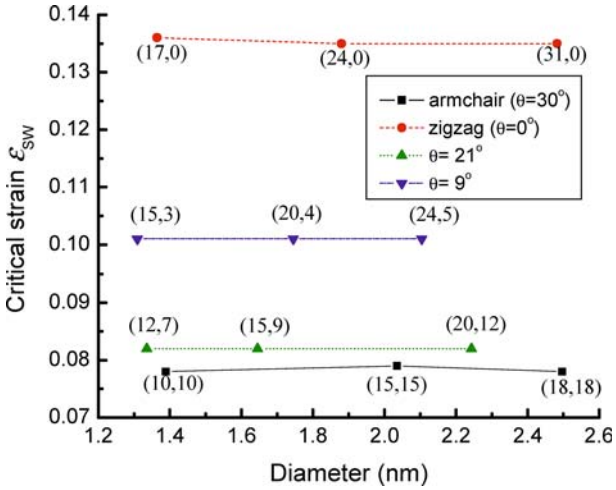

Figure 4. The dependence relation of the critical strains of defect nucleation upon the chiral angles and diameters of CNTs.

(i) (17, 0), (24, 0) and (31, 0), which are zigzag (i.e., the chiral angle $\theta = 0^\circ$);
(ii) (15, 3), (20, 4) and (24, 5), with the chiral angles being about $\theta = 9^\circ$;
(iii) (12, 7), (15, 9) and (20, 12), with the chiral angles being about $\theta = 21^\circ$;
(iv) (10, 10), (15, 15) and (18, 18), which are armchair (i.e., $\theta = 30^\circ$).

The calculation results of the critical strains of defect nucleation of CNTs are given in Figure 4, where the Young's modulus and Poisson's ratio of the matrix are taken as $E_m = 40\,\text{GPa}$ and $\nu_m = 0.2$, respectively. It is clear that the critical strain of a CNT is sensitive to its chiral angle but almost independent of its diameter. With the increase in the chiral angle, the critical strain decreases. The critical strain of defect nucleation of a zigzag CNT is about 13.6% and nearly twice that of an armchair CNT (about 7.8%). This is in agreement with the molecular dynamics simulation results of Nardelli et al. (1998). They considered CNTs at high temperature and not embedded in a composite, and found the critical strains are about 5% and 10% for armchair and zigzag CNTs, respectively.

3.2. Defect nucleation of CNTs in composites

Now we compare the critical strains of Stone–Wales defect nucleation of CNTs that are embedded in a composite and that are not embedded. An armchair CNT (10, 10) and a zigzag CNT (17, 0) are chosen as examples, whose diameters are almost the same. The elastic constants of the matrix are taken as the same as above. For the (10, 10) and (17, 0) CNTs, the changing curves of the averaged energy difference $\Delta E = E_{\text{defect}} - E_{\text{perfect}}$ over the region A are respectively given in Figure 5(a) and (b) with respect to the tensile strain. The solid and the dashed lines correspond to the CNTs that are embedded and not embedded in the composite, respectively. When ΔE reduces to zero, the Stone–Wales defect becomes favorable energetically. The critical strain of defect nucleation of the (10, 10) CNT is 7.5%, and becomes 7.8% after it is embedded in the composite. Similarly, the critical strain of the (17, 0) CNT increases from 13.2% to 13.6% after it is put into the composite. Due to the

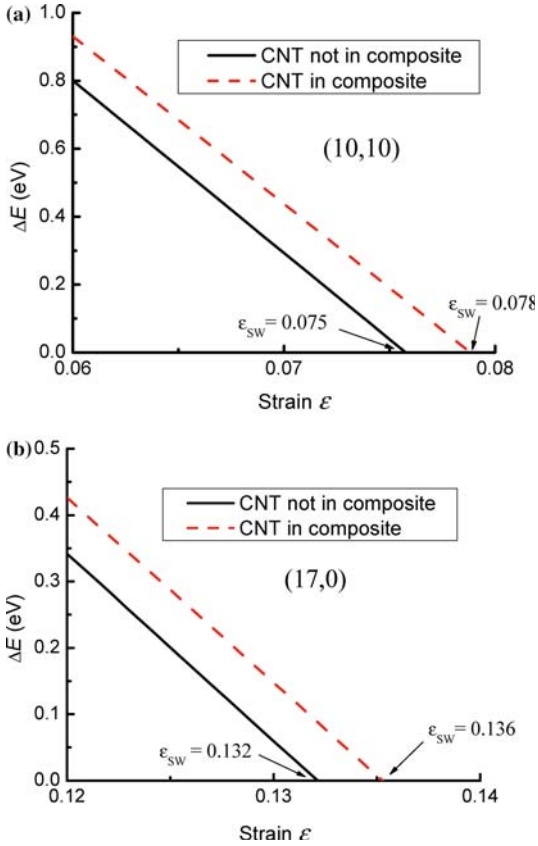

Figure 5. The averaged energy difference per atom over the region A with respect to the increasing tensile strain: (a) (10, 10) CNT, and (b) (17, 0) CNT.

constraint effect of matrix, therefore, Stone–Wales defects become more difficult to form in CNTs embedded in composites, though the change in the critical strain ε_{SW} is relatively small (less than 0.5%).

3.3. Fracture of CNTs in composites

The present method not only can predict the critical strain of Stone–Wales transformation, but also study the consequent defect evolution and fracture process of the CNT. After the nucleation of Stone–Wales defects, the deformation of the CNT is still stable until the breaking of a C—C bond. We simulated the deformation and fracture process after defect nucleation, and found that the deformation will become unstable and localized when the applied strain reaches a critical strain of breaking, ε_{break}. With the localization of deformation, some C—C bonds will become so long that their forces will become very weak according to the Tersoff–Brenner potential. It is generally thought (Brenner, 1990) that a C—C bond will break when the distance of the two atoms reaches 0.2 nm. Our simulations indicate that both the armchair and zigzag CNTs will break in the direction nearly normal to the tensile direction, as shown in the insets of Figure 6. The changing curves of energy with

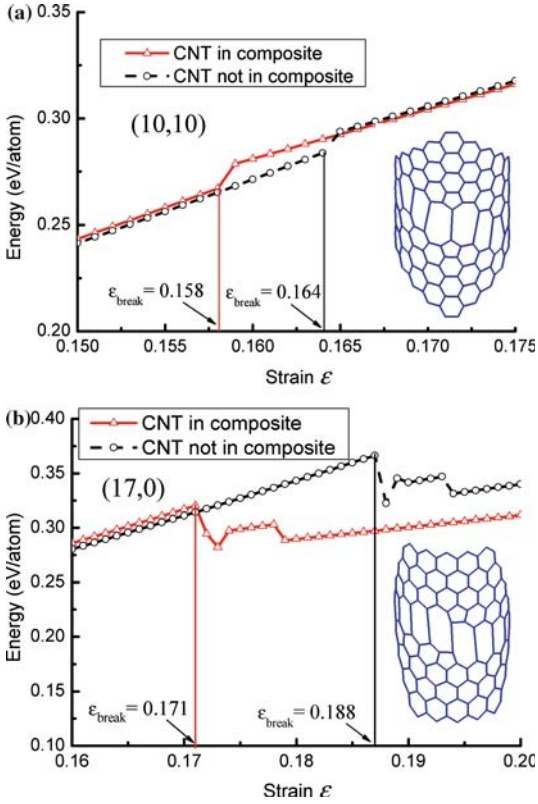

Figure 6. The changing curves of energy: (a) (10, 10) CNT, and (b) (17, 0) CNT.

defect evolution and fracture are plotted in Figure 6. The solid line corresponds to the CNTs embedded in the composite, and the dashed line corresponds to those not embedded. Corresponding to the deformation localization and breaking of a CNT, there is a rapid jump in the energy of the system, indicating the transformation from stable to unstable deformation.

It is also found that when a CNT is placed in a composite, its critical strain of breaking will decrease though its critical strain of defect nucleation increases. For example, the critical strain of fracture of the (10, 10) CNT is about 16.4%, and reduces to 15.8% after it is embedded in the composite. Similarly, the critical strain of breaking of the (17, 0) CNT decreases from 18.8% to 17.1% after it is put into the composite. This might also be attributed to the constraint effect of the matrix. A CNT embedded in a composite is less effective to release the energy, and becomes easier to fracture than that not embedded. In the present paper, we do not consider the fracture of the polymer matrix though in reality most polymers cannot sustain such a high tensile strain.

It is also seen that the deformation and fracture process of a CNT, either embedded in a composite or not, generally includes three stages, namely, the stable and uniform deformation of hexagonal lattice structure before Stone–Wales defect occurrence, the stable but nonuniform deformation after defect nucleation, and the unstable or localized deformation before the final fracture.

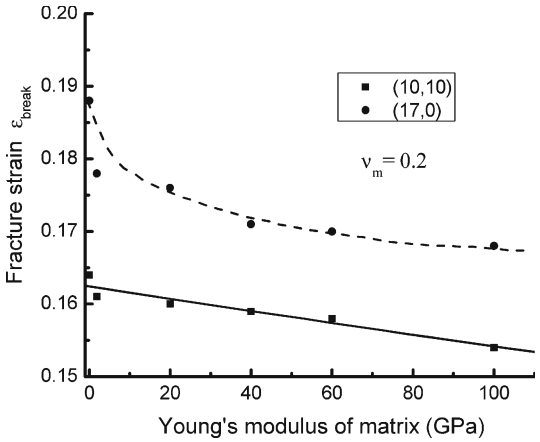

Figure 7. Breaking strains of (10, 10) and (17, 0) CNTs with respect to the Young's modulus of matrix.

3.4. Effect of matrix stiffness on CNT fracture

Finally, we examine how the stiffness of matrix influences the critical strains of fracture of CNTs. For (10, 10) and (17, 0) CNTs, the critical strains of fracture are shown in Figure 7 as a function of the Young's modulus of matrix. It is found that the breaking strain of CNTs decreases with the increases in the stiffness of matrix.

4. Conclusions

We have present a multiscale mechanics method to study the deformation and fracture of CNTs embedded in a composite. The unit cell for the CNT-reinforced composite is divided in three regions, which are simulated in a combined manner by the atomic-potential method, the atomistic-based continuum method, and the continuum mechanics, respectively. The critical strains of defect nucleation and breaking are calculated for some representative CNTs embedded in a composite. The influences of such factors as the chiral angle and diameter of CNTs as well as the elastic constant of matrix on the Stone–Wales defect formation and fracture behavior are investigated. The critical strain of defect nucleation of a CNT is sensitive to its chiral angle but not to its diameter. The constraint effect of matrix makes the CNTs easier to fracture.

Some other factor, e.g., the waviness of CNTs, the CNT–matrix interface adhesion, and the distributed residual stresses in composites, may influence the fracture behaviors of CNTs. The presented multiscale mechanics method can also be considered for accounting for these factors.

Acknowledgement

X.Q. Feng acknowledges the support from the National Natural Science Foundation of China (Grant No. 90305025 and 10121202), 973 Project (Grant No. 2004CB619303) and the Education Ministry of China (Grant No. 199926). Y. Huang acknowledges the support from ONR (Grant No. 00014-01-1-0205, Program Officer Dr. Y.D.S.

Yajakapse), NSF (Grants No. 0099909 and No. 0103257), Alexander von Humboldt Foundation, Center for Advanced Study at UIUC, NCSA Faculty Fellows Program, and NSFC.

References

Ajayan, P.M., Schadler, L.S., Giannaris, C. and Rubio, A. (2000). Single-walled nanotube-polymer composites: strength and weaknesses. *Advanced Materials* **12**, 750–753.

Andrews, R., Jacques, D., Rao, A.M., Rantell, T., Derbyshire, F. and Chen, Y. (1999). Nanotube composite carbon fibers. *Applied Physics Letters* **75**, 1329–1331.

Born, M. and Huang, K. (1954). *Dynamical Theory of Crystal Lattices*. Clarendon Press, Oxford.

Bower, C., Rosen, R. and Jin, L. (1999). Deformation of carbon nanotubes in nanotube-polymer composites. *Applied Physics Letters* **74**, 3317–3319.

Brenner, D.W. (1990). Empirical potential for hydrocarbons for use in simulation the chemical vapor deposition of diamond films. *Physical Review B* **42**, 9458–9471.

Buryachenko, V.A. and Roy, A. (2005). Effective elastic moduli of nanocomposites with prescribed random orientation of nanofibers. *Composites Part B:Engineering* **36**, 405–416.

Curtin, W.A. and Miller, R.E. (2003). Atomistic/continuum coupling in computational materials science. *Modeling and Simulation in Materials Science and Engineering* **11**, R33–R68.

Fisher, F.T., Bradshaw, R.D. and Brinson, L.C. (2002). Effects of nanotube waviness on the modulus of nanotube-reinforced polymers. *Applied Physics Letters* **80**, 4647–4649.

Ghoniem, N.M., Busso, E.P., Kioussis, N. and Huang, H.C. (2003). Multiscale modelling of nanomechanics and micromechanics: an overview. *Philosophical magazine* **83**, 3475–3528.

Hill, R. (1964). Theory of mechanical properties of fibre-strengthened materials: I. Elastic behaviour. *Journal of the Mechanics and Physics of Solids* **12**, 199–218.

Hu, N., Fukunaga, H., Lu, C., Kameyama, M. and Yan, B. (2005). Prediction of elastic properties of carbon nanotube reinforced composites. *Proceedings of Royal Society A*, **461**, 1685–1710.

Jiang, H., Zhang P., Liu, B., Huang, Y., Geubelle, P.H., Gao, H. and Hwang, K.C. (2003). The effect of nanotube radius on the constitutive model for carbon nanotubes. *Computational Materials Science* **28**, 429–442.

Jiang, H., Feng, X.Q., Huang,Y., Hwang, K.C. and Wu, P.D. (2004). Defect nucleation in carbon nanotubes under tension and torsion: Stone–Wales transformation. *Computer Methods in Applied Mechanics and Engineering* **193**, 3419–3429.

Liu, Y.J. and Chen, X.L. (2003). Evaluations of the effective material properties of carbon nanotube-based composites using a nanoscale representative volume element. *Mechanics of Materials* **35**, 69–81.

Lourie, O. and Wagner, H.D. (1999). Evidence of stress transfer and formation of fracture clusters in carbon nanotube-based composites. *Composites Science and Technology* **59**, 975–977.

Lourie, O., Cox, D.M. and Wagner, H.D. (1998). Buckling and collapse of embedded carbon nanotubes. *Physical Review Letters* **81**, 1638–1641.

Mori, T. and Tanaka, K. (1973). Average stress in matrix and average elastic energy of materials with misfitting inclusions. *Acta Metallurgica* **21**, 571–574.

Mura, T. (1987). *Micromechanics of Defects in Solids*. Martinus Nijhoff Publishers, The Netherlands.

Nardelli, M.B., Fattebert, J.L., Orlikowski, O., Roland, C., Zhao, Q. and Bernholc, J. (2000). Mechanical properties, defect and electronic behavior of carbon nanotubes. *Carbon* **38**, 1703–1711.

Nardelli, M.B., Yakobson, B.I. and Bernholc, J. (1998a). Brittle and ductile behavior in carbon nanotubes, *Physical Review Letters* **81**, 4656–4659.

Nardelli, M.B., Yakobson, B.I. and Bernholc, J. (1998b). Mechanism of strain release in carbon nanotubes. *Physical Review B* **57**, 4277–4280.

Odegard, G.M., Gates, T.S., Wise, K.E., Park, C. and Siochi, E.J. (2003). Constitutive modeling of nanotube-reinforced polymer composites. *Composites Science and Technology* **63**, 1671–1687.

Panhuis, M.I.H., Maiti, A., Dalton, A.B., van den Noort, A., Coleman, J.N., McCarthy, B. and Blau, W.J. (2003). Selective interaction in a polymer-single-wall carbon nanotube composite. *Journal of Physical Chemistry B* **107**, 478–482.

Pötschke, P., Fornes, T.D. and Paul, D.R. (2002). Rheological behavior of multiwalled carbon nanotube/polycarbonate composites. *Polymer* **43**, 3247–3255.

Qian, D., Dickey, E.C., Andrews, R. and Rantell, T. (2000). Load transfer and deformation mechanisms in carbon nanotube–polystyrene composites. *Applied Physics Letters* **74**, 3317–3319.

Ru, C.Q. (2001). Axially compressed buckling of a double-walled carbon nanotube embedded in an elastic medium. *Journal of the Mechanics and Physics of Solids* **49**, 1265–1279.

Ruan, S.L., Gao, P., Yang, X.G. and Yu, T.X. (2003). Toughening high performance ultrahigh molecular weight polyethylene using multiwalled carbon nanotubes. *Polymer* **44**, 5643–5654.

Schadler, L.S., Giannaris, S.C. and Ajayan, P.M. (1998). Load transfer in carbon epoxy composite. *Applied Physics Letters* **73**, 3842–3844.

Shenoy, V.B., Miller, R., Tadmor, E.B., Rodney, D., Phillips, R. and Ortiz, M. (1999). An adaptive finite element approach to atomic-scale mechanics – the quasicontinuum method. *Journal of the Mechanics and Physics of Solids* **47**, 611–642.

Shi, D.L., Feng, X.Q., Huang, Y. and Hwang, K.C. (2004a). Critical evaluation of the stiffening effect of carbon nanotubes in composites. *Key Engineering Materials* **261**–**263**, 1487–1492.

Shi, D.L., Feng, X.Q., Huang, Y., Hwang, K.C. and Gao, H. (2004b). The effect of nanotube waviness and agglomeration on the elastic property of carbon nanotube-reinforced composites. *Journal of Engineering Materials and Technology* **126**, 250–257.

Shi, D.L., Feng, X.Q., Jiang, H., Huang, Y. and Hwang, K.C. (2004c). A numerical study of fracture and defect nucleation in carbon nanotubes. *The 6th World Congress on Computational Mechanics (WCCM-VI)*, September 5–10, 2004, Beijing.

Tibbetts, G.G. and McHugh, J. (1999). Mechanical properties of vapor-grown carbon fiber composites with thermoplastic matrices. *Journal of Materials Research* **14**, 2871–2880.

Treacy, M.M.J. Ebbesen, T.W. and Gibson, J.M. (1996). Exceptionally high Young's modulus observed for individual carbon nanotubes. *Nature* **381**, 678–680.

Vigolo, B., Penicaud, A., Coulon, C., Sauder, C., Pailler, R. and Journet, C. (2000). Macroscopic fibers and ribbons of oriented carbon nanotubes. *Science* **290**, 1331–1334.

Wagner, H.D., Lourie, O., Feldman, Y. and Tenne, R. (1998). Stress-induced fragmentation of multiwall carbon nanotubes in a polymer matrix. *Applied Physics Letters* **72**, 188–190.

Watts, P.C.P. and Hsu, W.K. (2003). Behaviours of embedded carbon nanotubes during film cracking. *Nanotechnology* **14**, L7–L10.

Weng G.J. (1984). Some elastic properties of reinforced solids, with special reference to isotropic ones containing spherical inclusions. *International Journal of Engineering Science* **22**, 845–856.

Xia, Z., Riester, L., Curtin, W.A., Li, H., Sheldon, B.W., Liang, J., Chang, B. and Xu, J.M. (2003). Direct observation of toughening mechanisms in carbon nanotube ceramic matrix composites. *Acta Materialia* **52**, 931–944.

Yakobson, B.I. (1997). Dynamic topology and yield strength of carbon nanotubes. *Proceedings of the Symposium on Fullerenes* (Edited by R.S. Ruoff and K.M. Kadish), Electrochemical Society, Pennington, 549–560.

Yakobson, B.I. (1998). Mechanical relaxation and "intramolecular plasticity" in carbon nanotubes. *Applied Physics Letters* **72**, 918–920.

Yakobson, B.I., Brabec C.J. and Bernholc J. (1996). Nanomechanics of carbon tubes: instabilities beyond linear response. *Physical Review Letters* **76**, 2511–2514.

Yakobson, B.I., Campbell, M.P., Brabec, C.J. and Bernholc, J. (1997). High strain rate fracture and C-chain unraveling in carbon nanotubes. *Computational Materials Science* **8**, 341–348.

Yakobson, B.I. and Smalley, R.E. (1997). Fullerene nanotubes: $C_{1,000,000}$ and beyond. *American Scientist* **85**, 324–337.

Yu, M.F., Lourie, O., Dyer, M.J., Moloni, K., Kelly, T.F. and Ruoff, R.S. (2000). Strength and breaking mechanism of multiwalled carbon nanotubes under tensile load. *Science* **287**, 637–640.

Zhang, P., Huang, Y., Gao, H. and Hwang, K.C. (2002a). Fracture nucleation in single-wall carbon nanotubes under tension: a continuum analysis incorporating interatomic potentials. *Journal of Applied Mechanics* **69**, 454–458.

Zhang, P., Huang, Y., Geubelle, P.H., Klein, P.A. and Hwang, K.C. (2002b). The elastic modulus of single-wall carbon nanotubes: A continuum analysis incorporating interatomic potentials. *International Journal of Solids and Structures* **39**, 3893–3906.